
Systematic study for gas-to-dust ratio of short gamma-ray burst afterglows

Kazuki Yoshida^{*,†}, Daisuke Yonetoku^{*}, Makoto Arimoto, Tatsuya Sawano, Yasuaki Kagawa[†]

Faculty of Mathematics and Physics, Kanazawa University, Kakuma-machi, Kanazawa, Ishikawa 920-1192

*E-mail: yoshida@astro.s.kanazawa-u.ac.jp, yonetoku@astro.s.kanazawa-u.ac.jp

Received (reception date); Accepted (acceptation date)

Abstract

Extra-galactic X-ray absorption and optical extinction are often found in gamma-ray burst (GRB) afterglows and they could be tracers of both circumburst and host galaxy environments. By performing spectral analyses for spectral energy distribution of 9 short GRB (SGRB) afterglows with known redshift, we investigated a ratio of the equivalent hydrogen column density to the dust extinction, $N_{\text{H}}^{\text{rest}}/A_{\text{V}}^{\text{rest}}$, in the rest frame of each SGRB. We found that the distribution of $N_{\text{H}}^{\text{rest}}/A_{\text{V}}^{\text{rest}}$ is systematically smaller than the one for long GRBs, and is roughly consistent with the gas-to-dust ratio in the Milky Way. This result means that the measured gas-to-dust ratio of SGRBs would originate from the interstellar medium in each host galaxy. This scenario supports the prediction that SGRBs occur in non star-forming regions in the host galaxies.

Key words: gamma-ray burst: general — galaxies: ISM — dust, extinction

1 Introduction

Gamma-ray bursts (GRBs) are grouped in two classes based on their observed duration and spectral hardness of prompt emissions. Long GRBs (LGRBs) and short GRBs (SGRBs) typi-

[†] JSPS Research Fellow

cally have duration of longer and shorter than about 2 s, and relatively softer and harder spectra, respectively (e.g., Kouveliotou et al. 1993; Lien et al. 2016). LGRBs are almost always found in star-forming regions within star-forming galaxies (Bloom et al. 2002; Fruchter et al. 2006; Svensson et al. 2010), and their progenitors are confirmed as the death of massive stars (e.g., Hjorth et al. 2003; Woosley & Bloom 2006; Kumar & Zhang 2015, and references therein). On the other hand, some fraction of SGRBs occur in elliptical galaxies showing no star-formation (Fong et al. 2013; Fong & Berger 2013). The progenitors of SGRBs are considered to be the coalescence of binary neutron star (NS) and/or black hole (BH)-NS binary (e.g., Eichler et al. 1989; Narayan, Paczynski, & Piran 1992). In fact, the binary NS merger event, GW 170817, was observed through the gravitational waves by the LIGO and Virgo collaboration, which accompanied the SGRB candidate, GRB 170817A, (Abbott et al. 2017; Goldstein et al. 2017; Savchenko et al. 2017). Since the binary system should move away from their birth site until its merging by natal kicks in the compact binary merger scenario (e.g., Narayan, Paczynski, & Piran 1992; Bloom et al. 1999; Fryer et al. 1999; Belczynski et al. 2006), SGRBs may occur in non star-forming regions inside of host galaxies or outside of that. Therefore to investigate the surrounding environment of SGRBs and compare it with that of LGRBs are crucial way to interpret the SGRBs' progenitors.

To study the spectral energy distributions (SEDs) of GRB afterglows is the major approach to interpret surrounding environments of GRBs. GRB afterglows are thought to originate from relativistically expanding jets that form shocks between the jet and the surrounding medium (e.g., Rees & Mészáros 1992, 1998), and their SEDs in the optical to X-ray band can be described by a single or broken power-law function (Sari, Piran, & Narayan 1998; Granot & Sari 2002). Performing the spectral analysis for them, we can study extinction curves following SEDs and measure the amounts of X-ray absorption and optical extinction in the host galaxy, which are usually defined as an equivalent hydrogen column density (N_{H}) under the assumption of the solar abundance and an extinction in V band (A_{V}), respectively. The extinction curve shows the dependence of dust attenuation on wavelength, which originates from the dust size and their chemical properties and are different for galaxies, e.g., the Milky Way (MW), the Large Magellanic Cloud (LMC) and the Small Magellanic Cloud (SMC), (e.g., Pei 1992). The $N_{\text{H}}/A_{\text{V}}$ ratios, called gas-to-dust ratio¹, reflect the properties of the interstellar medium (ISM) in the galaxies and is considered to vary with galaxies, e.g. the MW, LMC and SMC (Welty et al. 2012).

¹ This is sometimes called metal-to-dust ratio, especially when the equivalent hydrogen column density is derived from the X-ray absorption, because the dominant X-ray absorbers are strictly metallic elements.

According to previous studies for afterglows of LGRBs (e.g., Schady et al. 2007, 2010; Covino et al. 2013), in the optical and near infrared (NIR) band, the extinction curve of the SMC well fits to SEDs of observation data rather than the one of the MW or LMC in almost all events. However, in the rest frame of each GRB, the ratio of hydrogen equivalent column density measured in X-ray band to the dust extinction measured in optical/NIR band ($N_{\text{H}}^{\text{rest}}/A_{\text{V}}^{\text{rest}}$) is significantly larger than the ones in the SMC as well as the MW and LMC. The dust destruction caused by the intense GRB emission is discussed as an major interpretation of the large $N_{\text{H}}^{\text{rest}}/A_{\text{V}}^{\text{rest}}$, but its observational evidence has been not found (Waxman & Draine 2000; Galama & Wijers 2001; Savaglio et al. 2003; Schady et al. 2010). Schady et al. (2010) reports the possibility that the $N_{\text{H}}/A_{\text{V}}$ ratio of LGRBs in low-metallicity galaxies is large. On the other hand, Zafar et al. (2011) investigated the $N_{\text{H}}^{\text{rest}}/A_{\text{V}}^{\text{rest}}$ ratio including metallicity of each LGRB in detail, but they concluded that only the metallicity can not explain the observed high $N_{\text{H}}^{\text{rest}}/A_{\text{V}}^{\text{rest}}$ ratio. Until now, a unified picture to explain such a large $N_{\text{H}}^{\text{rest}}/A_{\text{V}}^{\text{rest}}$ ratio has not been established.

In this paper, we systematically performed SED fitting for 9 SGRBs with known redshifts using both X-ray and optical/NIR afterglow data, and investigated the ratio of equivalent hydrogen column density to optical extinction of each GRB. Furthermore, we compared these ratio with the results of LGRBs and also typical galaxy environment. The error and upper/lower limits of all fitting parameters are shown at 68% and 90% confidence level, respectively.

2 Data reduction and analysis

We used SGRBs with known redshifts observed by the X-ray Telescope (XRT) on board the *Neil Gehrels Swift Observatory* (*Swift*) (Gehrels et al. 2004; Burrows et al. 2005). In addition to obvious SGRBs with $T_{90} < 2$ sec, we included possible SGRB candidates with $T_{90} > 2$ sec, which are considered as the SGRB with extended soft X-ray emissions following prompt emissions. Here T_{90} is the time duration which includes 90% of the observed photon counts except for the first and the last 5% in the GRB emission observed the *Swift*/BAT. We selected brighter 9 SGRBs, listed in Table 1, whose host galaxies were much dimmer than the optical/NIR afterglows.

Since the spectral parameters of the power-law index and the dust extinction in the SEDs of GRB afterglows are degenerate, we cannot correctly measure the dust extinction in the rest frame of SGRBs with only optical/NIR data, which are limited data points. Therefore, in order to obtain the reliable spectral parameters, we performed the simultaneous spectral

analysis for broadband SEDs consist of both optical/NIR and X-ray data, i.e. we estimate the spectral index in optical/NIR band including X-ray data. In Covino et al. (2013), the optical extinctions derived from only optical/NIR data analysis were consistent with those derived from the X-ray prior analysis as we mentioned.

2.1 Optical/NIR data

We gathered available data (not including upper limits) of optical/NIR afterglow observations from the published papers and GCN Circulars², and converted their magnitude to the flux density. The data we used and the references of them are listed in Table A.1. Using the database in the NASA/IPAC Infrared Science Archive³ (Schlafly & Finkbeiner 2011), we converted the observed flux density of each burst to the one before affecting the galactic extinction.

Since the GRB afterglow shows power-law decline in time (Sari, Piran, & Narayan 1998; Granot & Sari 2002), it is necessary to collect data at the same time as close as possible in order to create accurate SED. Here, we ignore the time difference among each band data observed almost at the same time (or slightly different time) when the relative uncertainty of the measured flux density ($\Delta F/F$) and the observation time ($\Delta t/t$) satisfies $\Delta F/F > \Delta t/t$. Since six of the nine samples satisfied the condition, we used the observation data of that epoch as the SEDs for these events. For the other three samples, GRB 070724A, 090510 and 140903A, we adopted a power-law function of $F(t) \propto (t - t_0)^{\alpha_{\text{opt}}}$ to the observed light curve in the same band, and we estimate the flux density at the time when the interpolation and extrapolation in all bands are minimized. Here, t_0 is the trigger time and α_{opt} is the temporal index in optical/NIR band. The time we set for each sample is summarized in Table 1.

2.2 X-ray data

X-ray observation data of SGRBs are taken from UK *Swift* Science Data Centre⁴. The XRT observation is generally performed in two modes, windowed timing (WT) and photon counting (PC) mode. The PC mode data as data of afterglows were used in this analysis, since the extended emission is often observed in the WT mode, whose origin is different from the one of afterglows (e.g., Norris & Bonnell 2006; Kagawa et al. 2015; Kisaka et al. 2017). The light-

² <https://gcn.gsfc.nasa.gov/>

³ <https://irsa.ipac.caltech.edu/applications/DUST/>

⁴ <http://www.swift.ac.uk/index.php>

curve data were taken from the XRT light curve repository⁵ (Evans et al. 2007, 2009). We extracted a source and background event data from circle region with 20 pixels and 40 in radius (corresponding to 47 and 94 arcsec), respectively, which are recommended ones in the *Swift* XRT Users Guide Version 1.2⁶. Using **XSELECT** software (v2.4)⁷, we extracted spectral data from the cleaned event data. For the spectral analysis, ancillary response files were created by **xrtmkarf** (v0.6.3) and response matrices were taken from the calibration database files⁸.

In Kagawa et al. (2019), they analyzed time-resolved X-ray spectra whose time intervals were divided to each spectrum contains 128 photons, and spectral parameters at each time were obtained. They also analyzed the time averaged spectra with all observation data in PC mode, and confirmed that the photon indices of both results are consistent with each other within the error. Thus we performed time averaged spectral analyses with the entire PC mode data to maximize a signal-to-noise ratio. The time averaged spectra were grouped to 20 counts per energy bin.

In order to determine the X-ray flux at any given time, we adopted the power-law function with the temporal index of X-ray band (α_X) to the X-ray light curves in the same way we did for optical/NIR light curves. Where light curve data were taken from the *Swift*-XRT lightcurve repository⁹, in which the systematic search of temporal breaks had been performed for light curves (Evans et al. 2007, 2009). Considering their results and excluding the time at the temporal breaks, we defined fitting intervals with simple power-laws. The fitting results are shown in Figure 1 as red solid lines. Using the best-fitting result, we estimated a conversion factor from average flux to the one of focusing time and renormalized the time-averaged X-ray spectra for the broadband SED analysis.

2.3 Spectral analysis

The spectral analysis is carried out with **XSPEC** software (v12.9.0)¹⁰ and fit models prepared in there. Based on a standard synchrotron shock model (Sari, Piran, & Narayan 1998; Granot & Sari 2002), we adopted a **powerlaw** model and **bknpower** model for the broadband SEDs. The X-ray spectral index (β_X) is derived from the photon index (Γ) of power-law in the relation

⁵ http://www.swift.ac.uk/xrt_curves/

⁶ <https://swift.gsfc.nasa.gov/analysis/>

⁷ <https://heasarc.gsfc.nasa.gov/docs/software/lheasoft/ftools/xselect/>

⁸ <https://heasarc.gsfc.nasa.gov/docs/heasarc/caldb/swift/>

⁹ http://www.swift.ac.uk/xrt_curves/

¹⁰ <https://heasarc.gsfc.nasa.gov/xanadu/xspec/>

of $\beta_X = 1 - \Gamma$. Then we imposed the spectral index of the optical/NIR region, $\beta_{\text{opt}} = \beta_X$ in the `powerlaw` model and $\beta_{\text{opt}} = \beta_X - 0.5$ in the `bknpower` model. The latter case corresponds to the condition where the cooling frequency of the synchrotron emission locates between the optical/NIR and X-ray ranges (Sari, Piran, & Narayan 1998; Granot & Sari 2002).

We added `phabs` and `zphabs` models corresponding to the photo-electric absorption in our galaxy and host galaxy, respectively. The parameter of the Galactic equivalent hydrogen column density ($N_{\text{H}}^{\text{gal}}$) is fixed to be the amount calculated for the sky coordinates of each SGRB by the database in the UK Swift Science Data Center¹¹ (Willingale et al. 2013), as shown in Table 1. The equivalent hydrogen column density in the host galaxy ($N_{\text{H}}^{\text{rest}}$) was derived from the model fit where the solar abundances were assumed. We note that the metallicity of the SGRB host galaxies show a wide value, but on the average, it is about a solar abundance (Berger 2014, and references therein).

To compute the extinctions in the host galaxy, we used the `zdust` model that considered extinction for wavelength by dust grains as described in Pei (1992). There are major three models of the extinction curves in the MW, LMC and SMC environments. We adopted all three extinction models and investigated the difference of extinction in each model. All results of our spectral analysis are summarized in Table 2, but in the Section 3, we reported the results of using the MW extinction model because there is little difference of the amount of optical extinction among the three models. In fact, the three extinction models are almost the same within the wavelength range of the observation data in the rest frame of 9 SGRBs.

3 Results

Figure 1 shows the optical/NIR and X-ray light curves and the epoch of the broadband SED of each GRB. Although the time when the multi-band observation was performed for GRB 050724 is in the X-ray flare phase, we set this epoch for the broadband SED because it is reported in Berger et al. (2005) (see also Malesani et al. 2007) that the optical/NIR and X-ray emission might belong to the same component. In GRB 150423A, there are two times with multi-band observation data, i.e an early epoch (~ 240 s) and a later one (~ 15300 s). Since the extended emission was observed in the early epoch (Kisaka et al. 2017; Kagawa et al. 2019), we selected the later epoch.

The broadband SEDs with best-fit models are shown in Figure 2 and the results of our spectral analyses are summarized in Table 2 (see also Table A.2). For the SEDs of two SGRBs

¹¹<http://www.swift.ac.uk/analysis/nhtot/index.php>

(GRB 130603B, 150424A), the broken power-law models have better fitting results rather than the single power-law model. These are consistent with the previous studies (de Ugarte Postigo et al. 2014; Knust et al. 2017).

Figure 3 shows a scatter plot between $N_{\text{H}}^{\text{rest}}$ and $A_{\text{V}}^{\text{rest}}$ of SGRBs (this work) and LGRBs (Covino et al. 2013), and the typical gas-to-dust ratio of the MW, $N_{\text{H}}/A_{\text{V}} = 1.9 \times 10^{21} \text{ cm}^{-2} \text{ mag}^{-1}$ (Welty et al. 2012). As shown in Figure 3, we found that the $N_{\text{H}}^{\text{rest}}/A_{\text{V}}^{\text{rest}}$ ratio in the rest frame of SGRBs is systematically smaller than the one of LGRBs, and is roughly consistent with the gas-to-dust ratio in the MW.

4 Discussion

In order to investigate the selection effect on $N_{\text{H}}^{\text{rest}}$, we analyzed X-ray afterglow spectra of all 20 SGRBs (not including our 9 samples) with known redshift observed by *Swift*/XRT before the end of 2017, which did not have any near simultaneous optical/NIR data. We performed the spectral analysis for each time-averaged spectrum consists of observation data in PC mode. The sample and the fitting result are listed in Table 3. Figure 4 shows the histograms of the best fit value of $N_{\text{H}}^{\text{rest}}$ for our initial 9 samples and additional 20 samples. We created the cumulative distribution of best fit $N_{\text{H}}^{\text{rest}}$ and applied the Kolmogorov-Smirnov test to it. Then, we found the null hypothesis probability of 0.79 and our 9 samples show the same $N_{\text{H}}^{\text{rest}}$ distribution of the other 20 SGRBs. Therefore we concluded the $N_{\text{H}}^{\text{rest}}$ of our 9 SGRBs are not affected by the selection bias, while we cannot give further argument on the selection bias in $A_{\text{V}}^{\text{rest}}$ under the limited observation data. Since Krühler et al. (2011) reports the anti-correlation between the $A_{\text{V}}^{\text{rest}}$ and the $N_{\text{H}}^{\text{rest}}/A_{\text{V}}^{\text{rest}}$ ratio for LGRBs, the selection bias in $A_{\text{V}}^{\text{rest}}$ should be discussed in detail for future observation data of SGRBs.

In our 9 SGRB samples, the measured gas-to-dust ratio of SGRBs is roughly close to the one of the MW. Our result means that a major contribution of both extinction in optical/NIR band and absorption in X-ray band originates from the ISM in the host galaxy of SGRB. In other words, most of SGRBs are likely to occur in not star-forming regions but typical ISM environments of galaxies such as the MW. This result on the environment is consistent with the scenario that the coalescence of the compact binaries are the origin of because the system must move away from the location of their birth by natal kicks until its merging (e.g., Narayan, Paczynski, & Piran 1992; Bloom et al. 1999; Fryer et al. 1999; Belczynski et al. 2006).

$N_{\text{H}}^{\text{rest}}$ will show the amount of the intervening ISM within the host galaxy. In our results, we found approximately half of SGRB samples show $N_{\text{H}}^{\text{rest}}$ to be consistent with zero

while we obtained only marginal upper limit on them. These SGRBs are considered to occur in outskirts or outside of the host galaxies in which there are almost no X-ray absorption (and dust extinction) by the ISM. Moreover, while GRB 170817A with GW 170817, whose origin is the binary neutron star merger (Abbott et al. 2017; Goldstein et al. 2017; Savchenko et al. 2017), which occurred at only $1 r_e$ from the center of the host galaxy. Here r_e is given by a Sérsic model (Ciotti & Bertin 1999). However the X-ray absorption and optical extinction in the host galaxy are not significantly detected (Levan et al. 2017; Pooley et al. 2018). This event might occur at the location apart from the host galaxy toward the observer’s side. The $N_{\text{H}}^{\text{rest}}$ value might be an indicator of the offset along the line of sight.

Acknowledgments

We gratefully thank the anonymous referee for quick responses and helpful comments, and we also acknowledge the quick and kind responses of the editors. We also thank Yuu Niino for useful discussions. This work made use of data supplied by the UK Swift Science Data Centre at the University of Leicester, and is supported by JSPS KAKENHI Grant Number JP17J00905 (KY), JP16H06342 (DY), JP18J13042 (YK), MEXT KAKENHI Grant Number JP18H04580 (DY), JP17H06362 (MA), and Sakigake 2018 Project of Kanazawa University (DY). MA acknowledges the support from the JSPS Leading Initiative for Excellent Young Researchers program.

Table 1. Samples of SGRBs.

GRB	z	$N_{\text{H}}^{\text{gal}}$ (10^{20} cm^{-2})	$A_{\text{V}}^{\text{gal}}$ (mag)	Epoch (s)
050724	0.258	27.7	1.61	41783
051221A	0.5465	7.52	0.18	184701
070724A	0.457	1.21	0.04	10872
090510	0.903	1.77	0.05	28267
130603B	0.3564	2.1	0.06	52714
140903A	0.351	3.26	0.09	47117
150423A	1.394	1.77	0.08	15300
150424A	0.3	6.02	0.16	57903
170428A	0.454	6.95	0.16	3660

Table 2. Results of spectral analysis.

GRB	$N_{\text{H}}^{\text{rest}}$ (10^{21} cm^{-2})	$A_{\text{V}}^{\text{rest}}$ (mag)	β_{X}	E_{bk} (eV)	χ^2 (dof)	Null hypothesis probability
050724	< 0.21	< 0.12	$-0.74^{+0.01}_{-0.01}$	–	40 (31)	0.121
051221A	$0.56^{+0.31}_{-0.29}$	$0.81^{+0.37}_{-0.36}$	$-0.83^{+0.06}_{-0.06}$	–	44 (46)	0.544
070724A	$4.03^{+0.73}_{-0.63}$	$1.89^{+0.31}_{-0.30}$	$-0.77^{+0.02}_{-0.02}$	–	23 (19)	0.226
090510	$1.53^{+0.28}_{-0.26}$	$0.07^{+0.07}_{-0.07}$	$-0.84^{+0.02}_{-0.02}$	–	107 (85)	0.051
130603B	$2.99^{+0.30}_{-0.36}$	$1.14^{+0.10}_{-0.10}$	$-0.98^{+0.08}_{-0.07}$	8^{+19}_{-6}	48 (49)	0.498
140903A	$1.53^{+0.31}_{-0.28}$	$0.79^{+0.23}_{-0.24}$	$-0.80^{+0.03}_{-0.03}$	–	49 (39)	0.128
150423A	$1.59^{+1.50}_{-1.17}$	< 0.55	$-0.76^{+0.03}_{-0.03}$	–	6 (7)	0.536
150424A	$0.32^{+0.23}_{-0.22}$	< 0.15	$-1.01^{+0.07}_{-0.07}$	59^{+82}_{-34}	66 (46)	0.027
170428A	< 2.55	< 0.09	$-0.73^{+0.03}_{-0.02}$	–	8 (7)	0.344

Table 3. Samples of additional 20 SGRBs.

GRB	z	$N_{\text{H}}^{\text{gal}}$ (10^{20} cm^{-2})	$N_{\text{H}}^{\text{rest}}$ (10^{21} cm^{-2})
060614	0.125	2.09	$0.11_{-0.01}^{-0.01}$
060801	1.131	1.45	< 1.4
061006	0.4377	25.1	< 2.3
061201	0.111	6.8	< 0.32
070714B	0.923	9.82	$0.87_{-0.57}^{+0.62}$
070809	0.2187	8.62	< 1.1
071227	0.383	1.31	< 3.0
080123	0.495	2.52	< 1.7
080905	0.121	13.5	$1.28_{-0.77}^{+0.91}$
090426	2.609	1.58	< 3.0
090530	1.266	1.84	$2.20_{-0.76}^{+0.81}$
100117A	0.915	2.97	$1.11_{-0.97}^{+1.13}$
100625A	0.453	2.23	< 0.66
100816A	0.804	5.70	$1.24_{-0.57}^{+0.63}$
101219A	0.718	5.91	$4.39_{-3.35}^{+3.69}$
111117A	2.211	4.12	$17.5_{-8.1}^{+9.8}$
160228A	1.64	8.98	< 11
160410A	1.717	1.8	< 11
160624A	0.483	9.31	< 17
160821B	0.16	5.95	< 0.53

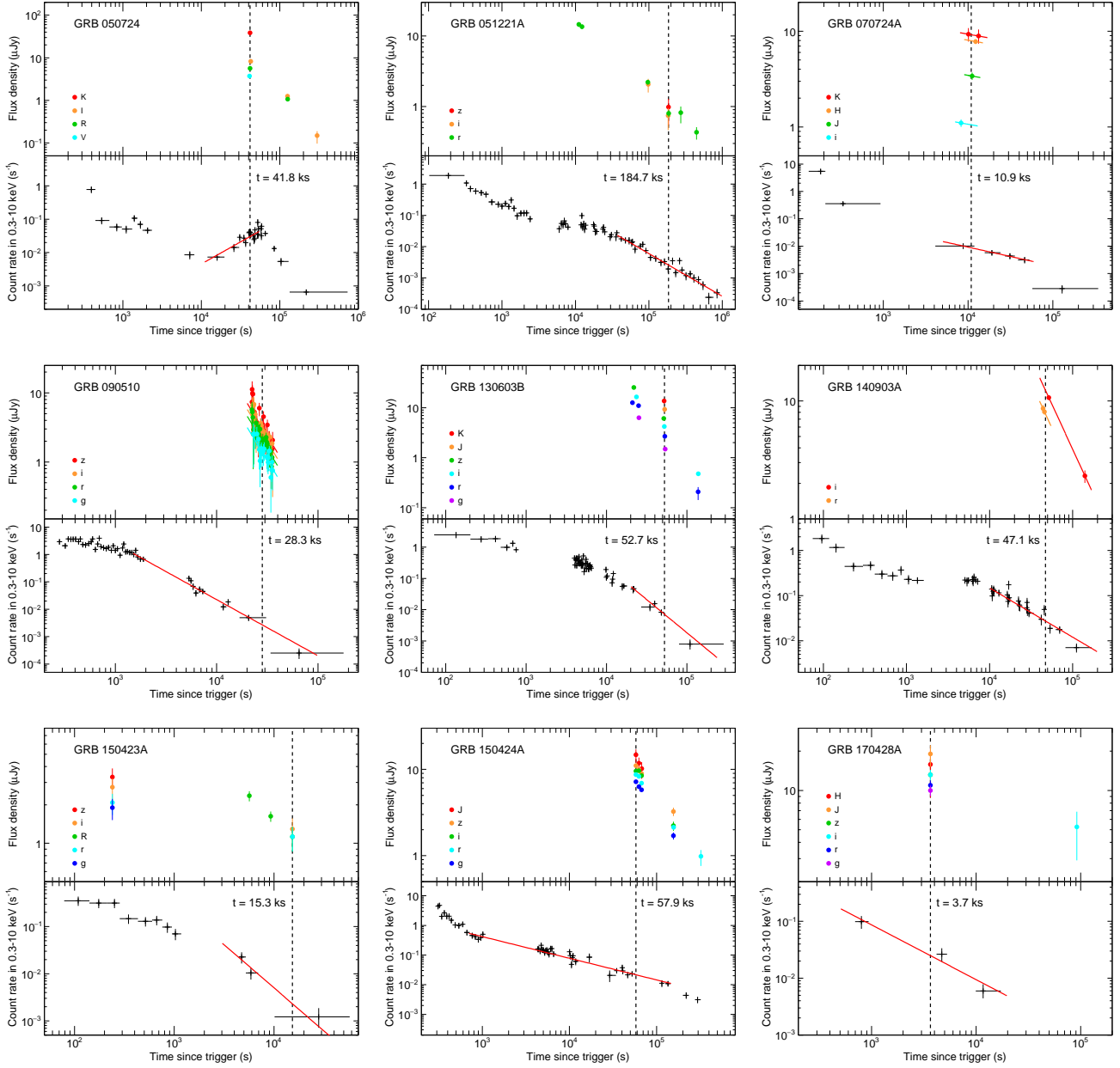


Fig. 1. Optical/NIR and X-ray light curves in the observer frame. The solid lines and the vertical dashed lines show the best-fit power-law models of each observation band and the epoch of broadband SEDs of each SGRB, respectively.

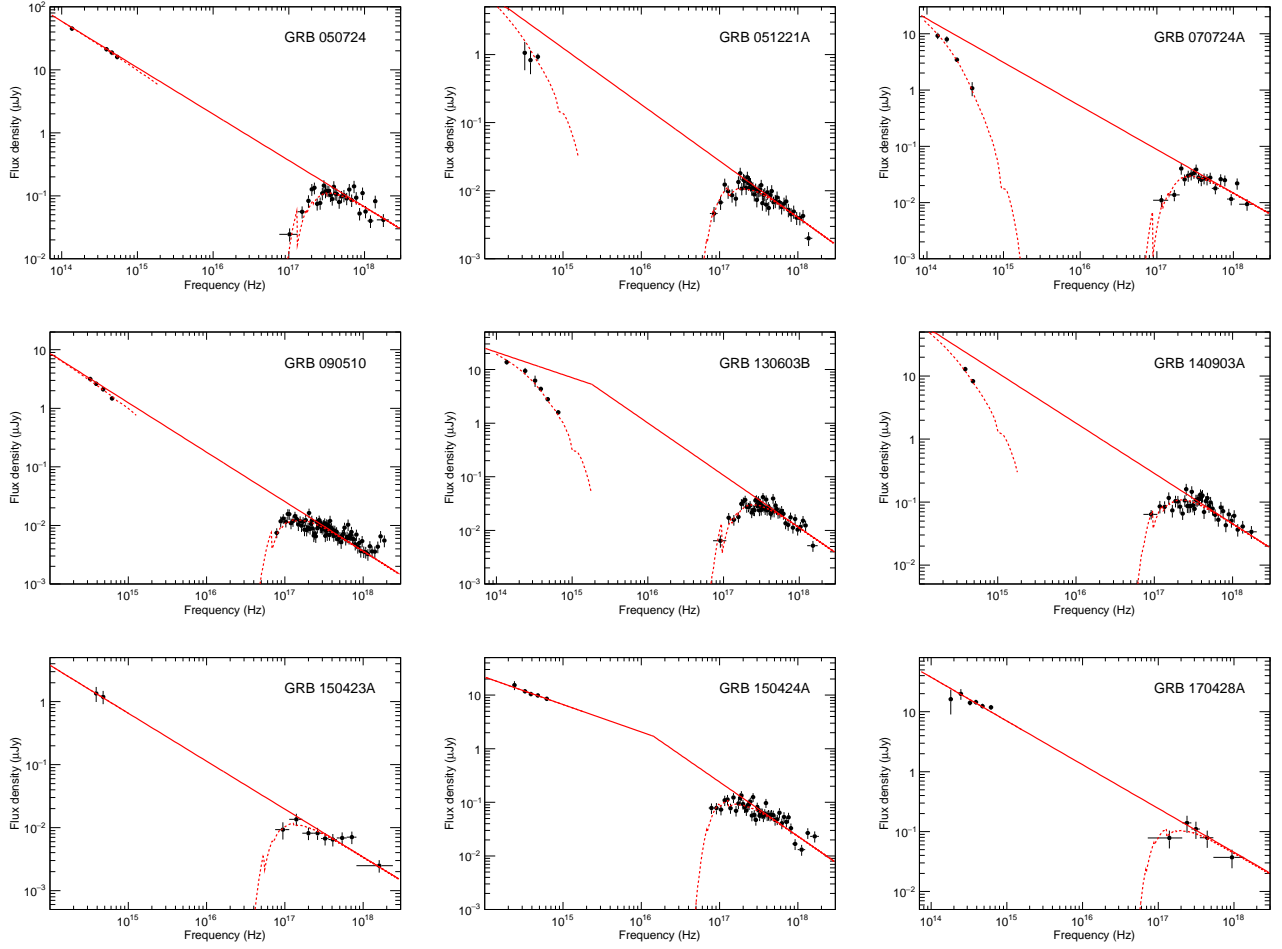


Fig. 2. The spectral energy distribution of 9 SGRBs. The optical/NIR data points are corrected for Galactic extinction, but the X-ray data points are not corrected for Galactic absorption. The solid lines show the best-fit unabsorbed spectral model corrected absorption and extinction. The dashed lines show the best-fit absorbed model including the Galactic and host-galactic absorption, and host-galactic extinction.

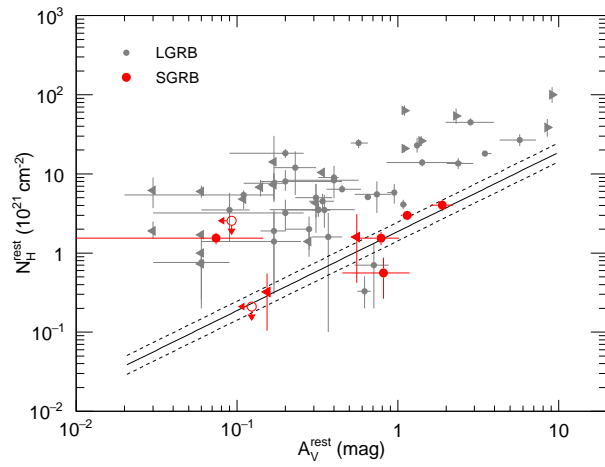


Fig. 3. Rest-frame column density versus rest-frame extinction. The red and gray points are our result in this paper and the ones of LGRBs by Covino et al. (2013). The triangles are the upper limits at 90% confidence level. The solid and dashed lines show the typical gas-to-dust ratio for the Milky Way and the corresponding 1σ uncertainty (Welty et al. 2012).

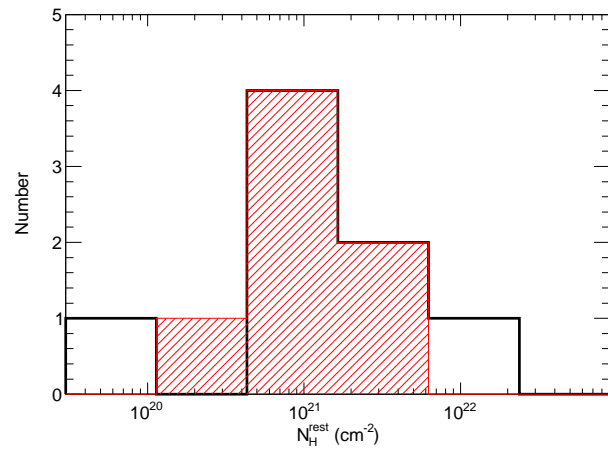


Fig. 4. Histograms of the equivalent hydrogen column density in the GRB rest frame. The black and red lines show the distribution of our 9 SGRBs and additional 20 SGRBs, respectively.

References

- Abbott, B., et al. 2017, ApJL, 848, L12
- Belczynski, K., et al. 2006, ApJ, 648, 1110
- Berger, E., et al. 2005, Nature, 438, 988
- Berger, E., Cenko, S. B., Fox, D. B., & Cucchiara, A. 2009, ApJ, 704, 877
- Berger, E., 2014, ARA&A, 52, 43
- Bloom, J. S, Sigurdsson, S., & Pols, O. 1999, MNRAS, 305, 763
- Bloom, J. S, Kulkarni, S. R., & Djorgovski, S. G. 2002, AJ, 123, 1111
- Bolmer, J., Steinle, H., & Schady, P. 2017, GCN Circ., 21050
- Burrows, D., et al. 2005, Space Sci. Rev., 120, 165
- Ciotti, L., & Bertin, G. 1999, *ã*, 352, 447
- Covino, S., et al. 2013, MNRAS, 432, 1231
- de Ugarte Postigo, A., et al. 2014, A&A, 563, A62
- Galama, T. J., & Wijers, R. A. M. J. 2001, ApJL, 549, L209
- Gehrels, N., et al. 2004, ApJ, 611, 1005
- Goldstein, A., et al. 2017, ApJL, 848, L14
- Eichler, D., Livio, M., Schramm, D. N., et al. 1989, Nature, 340, 126
- Evans, P. A., et al. 2007, *ã*, 469, 379
- Evans, P. A., et al. 2007, MNRAS, 397, 1177
- Fong, W., et al. 2013, apj, 769, 56
- Fong, W., & Berger, E. 2013, apj, 776, 16
- Fong, W., Berger, E., Margutti, R., & Zauderer, B. A. 2015, ApJ, 815, 102
- Fruchter, A. S, et al. 2006, Nature, 441, 463
- Fryer, C., Woosley, S., & Hartman, D. 1999, ApJ, 526, 152
- Granot, J., & Sari R. 2002, ApJ, 568, 820
- Guelbenzu, A. N., et al. 2012, A&A, 538, L7
- Hjorth, J., et al. 2003, Nature, 423, 847
- Kagawa, Y., et al. 2015, ApJ, 811, 4.
- Kagawa, Y., et al. 2019, ApJ, in prep.
- Kann, D. A. 2015, GCN Circ., 17738
- Kisaka, S., Ioka, K., & Sakamoto, T. 2017, ApJ, 846, 142K
- Knust, F., et al. 2017, A&A, 607, A84
- Kouveliotou, C., et al. 1993, ApJ, 413L, 101K
- Krühler, T., et al. 2011, A&A, 534, A108

Kumar, P., & Zhang, B. 2015, *Phys. Rep.*, 561, 1
Levan, A., J., et al. 2017, *ApJ*, 848, L28
Lien, A., et al. 2016, *ApJ*, 829, 7
Littlejohns, O., et al. 2015, *GCN Circ.*, 17736
Malesani, D., et al. 2007, *A&A*, 473, 77
Narayan, R., Paczynski, B., Piran, T. 1992, *ApJ*, 395, L83
Norris, J. P., & Bonnell, J. T. 2006, *ApJ*, 643, 266
Pei, Y. C., 1992, *ApJ*, 395, 130
Pooley, D., Kumar, P., Wheeler, J., C., & Grossan, B. 2018, *ApJ*, 859, L23
Rees, M. J., Mészáros, P. 1992, *MNRAS*, 258, 41
Rees, M. J., Mészáros, P. 1998, *ApJ*, 496, L1
Sari, R., Piran, T., & Narayan, R. 1998, *ApJL*, 497, L17
Savchenko, V., et al. 2017, *ApJ*, 848, L15
Savaglio, S., Fall, S. M., & Fiore, F. 2003, *ApJ*, 585, 638
Schady, P., et al. 2007, *MNRAS*, 377, 273
Schady, P., et al. 2010, *MNRAS*, 401, 2773
Schlafly, E. F., & Finkbeiner, D. P. 2011, *ApJ*, 737, 103
Svensson, K. M., Levan, A. J., Tanvir, N. R., Fruchter, A. S., & Strolger, L.-G. 2010, *MNRAS*, 405,
57
Soderberg, A. M., et al. 2006, *ApJ*, 650, 261
Troja, W., et al. 2016, *ApJ*, 827, 102
Troja, E., et al. 2017, *GCN Circ.*, 21051
Varela, K., & Berger, E. 2015, *GCN Circ.*, 17732
Waxman, E., & Draine, B. T. 2000, *apj*, 537, 796
Welty, D. E., Xue, R., & Wong, T. 2012, *ApJ*, 745, 173
Willingale, R., et al. 2013, *MNRAS*, 431, 394
Woosley, S. E., & Bloom, J. S. 2006, *ARA&A*, 44, 507
Zafar, T., et al. 2011, *A&A*, 532, A143

Appendix 1 Optical/NIR observation data and result of spectral analysis

Table A.1: Optical/NIR observation data of our sample

GRB	Filter	δt^1 (sec)	Flux ² (μ Jy)	Reference ³
050724	<i>K</i>	41760	$38.7^{+1.4}_{-1.4}$	(a)
	<i>I</i>	42517	$8.2^{+0.2}_{-0.2}$	(b)
		125420	$1.3^{+0.1}_{-0.1}$	(b)
		298980	$0.15^{+0.05}_{-0.04}$	(b)
	<i>R</i>	41797	$5.7^{+0.2}_{-0.2}$	(b)
		126160	$1.1^{+0.1}_{-0.1}$	(b)
	<i>V</i>	41070	$3.7^{+0.1}_{-0.1}$	(b)
	051221A	<i>z</i>	184697	$0.98^{+0.44}_{-0.30}$
<i>i</i>		97986	$2.1^{+0.5}_{-0.4}$	(c)
		183522	$0.74^{+0.28}_{-0.21}$	(c)
<i>r</i>		11120	$14.6^{+1.1}_{-1.0}$	(c)
		12277	$13.6^{+1.0}_{-1.0}$	(c)
		97001	$2.2^{+0.2}_{-0.2}$	(c)
		185890	$0.80^{+0.09}_{-0.08}$	(c)
		272419	$0.82^{+0.24}_{-0.19}$	(c)
	445116	$0.43^{+0.09}_{-0.08}$	(c)	
070724A ⁴	<i>K</i>	10080	$9.3^{+1.5}_{-1.5}$	(d)
		13320	$8.9^{+1.5}_{-1.5}$	(d)
	<i>H</i>	12240	$7.8^{+0.4}_{-0.4}$	(d, e)
	<i>J</i>	11160	$3.4^{+0.3}_{-0.3}$	(d, e)
	<i>i</i>	8280	$1.1^{+0.1}_{-0.1}$	(d)
090510	<i>z</i>	22299	$7.4^{+5.0}_{-3.0}$	(f)
		22401	$11.3^{+5.0}_{-3.5}$	(f)
		22609	$9.9^{+4.4}_{-3.1}$	(f)
		22743	$9.5^{+2.8}_{-2.2}$	(f)
		23639	$5.3^{+1.8}_{-1.4}$	(f)
		24093	$4.0^{+2.0}_{-1.4}$	(f)
		24984	$3.6^{+1.4}_{-1.0}$	(f)
		25889	$2.4^{+1.2}_{-0.8}$	(f)
	26335	$6.0^{+1.4}_{-1.2}$	(f)	

Table A.1: continued

GRB	Filter	δt^1 (sec)	Flux ² (μ Jy)	Reference ³
		27234	$3.5^{+1.1}_{-0.8}$	(f)
		28125	$2.6^{+1.0}_{-0.7}$	(f)
		28569	$3.2^{+1.1}_{-0.8}$	(f)
		29024	$4.5^{+1.1}_{-0.9}$	(f)
		29475	$2.8^{+1.3}_{-0.9}$	(f)
		30375	$2.3^{+1.0}_{-0.7}$	(f)
		30831	$2.4^{+1.3}_{-0.8}$	(f)
		31725	$3.4^{+0.8}_{-0.7}$	(f)
		32628	$1.9^{+1.0}_{-0.7}$	(f)
		33077	$2.3^{+0.7}_{-0.5}$	(f)
		35270	$1.5^{+0.7}_{-0.5}$	(f)
		35715	$2.1^{+0.9}_{-0.7}$	(f)
	<i>i</i>	22609	$6.6^{+2.9}_{-2.0}$	(f)
		22931	$5.0^{+2.1}_{-1.5}$	(f)
		23127	$6.5^{+2.5}_{-1.8}$	(f)
		23313	$6.9^{+2.5}_{-1.8}$	(f)
		23639	$4.2^{+1.4}_{-1.0}$	(f)
		24093	$4.9^{+1.0}_{-0.8}$	(f)
		24540	$2.8^{+1.4}_{-0.9}$	(f)
		24984	$3.5^{+1.3}_{-0.9}$	(f)
		25443	$2.6^{+1.1}_{-0.8}$	(f)
		25889	$2.3^{+1.1}_{-0.7}$	(f)
		26780	$2.0^{+0.6}_{-0.4}$	(f)
		27234	$3.6^{+0.7}_{-0.6}$	(f)
		27679	$3.4^{+0.6}_{-0.5}$	(f)
		28125	$2.7^{+0.7}_{-0.6}$	(f)
		28569	$2.9^{+0.8}_{-0.6}$	(f)
		29024	$2.7^{+0.7}_{-0.6}$	(f)
		29475	$2.4^{+0.7}_{-0.6}$	(f)
		29922	$2.3^{+0.8}_{-0.6}$	(f)

Table A.1: continued

GRB	Filter	δt^1 (sec)	Flux ² (μ Jy)	Reference ³
		30375	$2.2^{+0.7}_{-0.5}$	(f)
		30831	$2.5^{+0.8}_{-0.6}$	(f)
		31275	$1.9^{+0.4}_{-0.3}$	(f)
		31725	$2.1^{+0.4}_{-0.4}$	(f)
		32170	$1.3^{+0.6}_{-0.4}$	(f)
		32628	$2.3^{+0.7}_{-0.5}$	(f)
		33077	$1.8^{+0.6}_{-0.4}$	(f)
		33524	$2.3^{+0.3}_{-0.3}$	(f)
		34369	$1.1^{+0.7}_{-0.4}$	(f)
		35270	$1.9^{+0.6}_{-0.4}$	(f)
		35715	$1.0^{+0.7}_{-0.4}$	(f)
	<i>r</i>	22299	$5.7^{+2.4}_{-1.7}$	(f)
		22503	$5.3^{+2.2}_{-1.6}$	(f)
		22743	$4.4^{+1.6}_{-1.2}$	(f)
		22931	$2.5^{+1.8}_{-1}$	(f)
		23127	$2.9^{+1.8}_{-1.1}$	(f)
		23313	$2.5^{+1.6}_{-1.0}$	(f)
		24093	$2.2^{+0.7}_{-0.5}$	(f)
		24540	$3.7^{+0.7}_{-0.6}$	(f)
		24984	$2.6^{+0.9}_{-0.6}$	(f)
		25443	$3.3^{+0.8}_{-0.6}$	(f)
		25889	$2.8^{+0.7}_{-0.6}$	(f)
		26335	$2.1^{+0.7}_{-0.5}$	(f)
		26780	$3.0^{+0.7}_{-0.6}$	(f)
		27234	$2.2^{+0.6}_{-0.4}$	(f)
		27679	$1.8^{+0.4}_{-0.3}$	(f)
		28125	$1.9^{+0.5}_{-0.4}$	(f)
		28569	$2.1^{+0.5}_{-0.4}$	(f)
		29024	$1.7^{+0.6}_{-0.4}$	(f)
		29475	$2.0^{+0.5}_{-0.4}$	(f)

Table A.1: continued

GRB	Filter	δt^1 (sec)	Flux ² (μ Jy)	Reference ³
		29922	$1.9_{-0.4}^{+0.5}$	(f)
		30375	$2.1_{-0.4}^{+0.4}$	(f)
		30831	$2.3_{-0.4}^{+0.5}$	(f)
		31275	$1.9_{-0.4}^{+0.5}$	(f)
		31725	$1.8_{-0.3}^{+0.4}$	(f)
		32170	$1.5_{-0.3}^{+0.5}$	(f)
		32628	$1.6_{-0.3}^{+0.4}$	(f)
		33077	$1.2_{-0.3}^{+0.4}$	(f)
		33524	$1.4_{-0.3}^{+0.4}$	(f)
		34369	$1.4_{-0.3}^{+0.4}$	(f)
		34815	$0.86_{-0.30}^{+0.45}$	(f)
		35270	$1.2_{-0.3}^{+0.4}$	(f)
	<i>g</i>	23127	$2.6_{-1.0}^{+1.7}$	(f)
		23639	$2.5_{-0.7}^{+1.0}$	(f)
		24984	$2.6_{-0.7}^{+0.9}$	(f)
		25889	$2.1_{-0.5}^{+0.7}$	(f)
		26335	$1.5_{-0.5}^{+0.7}$	(f)
		26780	$1.0_{-0.4}^{+0.6}$	(f)
		27234	$1.4_{-0.4}^{+0.6}$	(f)
		27679	$1.6_{-0.3}^{+0.4}$	(f)
		28125	$1.3_{-0.3}^{+0.5}$	(f)
		29024	$1.4_{-0.4}^{+0.5}$	(f)
		29475	$1.5_{-0.4}^{+0.5}$	(f)
		31275	$1.2_{-0.3}^{+0.4}$	(f)
		31725	$1.1_{-0.3}^{+0.4}$	(f)
		32170	$0.99_{-0.25}^{+0.33}$	(f)
		32628	$1.1_{-0.3}^{+0.4}$	(f)
		33077	$1.4_{-0.3}^{+0.3}$	(f)
		34369	$0.60_{-0.24}^{+0.41}$	(f)
		34815	$0.77_{-0.19}^{+0.25}$	(f)

Table A.1: continued

GRB	Filter	δt^1 (sec)	Flux ² (μJy)	Reference ³
		35270	$1.0^{+0.3}_{-0.3}$	(f)
		35715	$0.75^{+0.37}_{-0.25}$	(f)
130603B	<i>K</i>	52099	$13.7^{+1.5}_{-1.3}$	(g)
	<i>J</i>	53050	$9.3^{+1.3}_{-1.1}$	(g)
	<i>z</i>	21946	$25.4^{+1.4}_{-1.4}$	(g)
		51754	$6.1^{+0.2}_{-0.2}$	(g)
	<i>i</i>	23674	$16.4^{+0.9}_{-0.9}$	(g)
		52445	$4.2^{+0.1}_{-0.1}$	(g)
	<i>r</i>	21082	$12.6^{+0.2}_{-0.2}$	(g)
		25056	$11.0^{+0.2}_{-0.2}$	(g)
		53136	$2.7^{+0.1}_{-0.1}$	(g)
		138240	$0.21^{+0.07}_{-0.05}$	(g)
	<i>g</i>	25402	$6.3^{+0.4}_{-0.3}$	(g)
		53827	$1.5^{+0.1}_{-0.1}$	(g)
140903A	<i>i</i>	51840	$10.7^{+0.5}_{-0.5}$	(h)
		140832	$2.3^{+0.3}_{-0.3}$	(h)
	<i>r</i>	44064	$8.6^{+0.7}_{-0.6}$	(h)
		45792	$8.1^{+0.5}_{-0.4}$	(h)
150423A	<i>z</i>	240	$3.3^{+0.7}_{-0.6}$	(i)
	<i>i</i>	240	$2.8^{+0.6}_{-0.5}$	(i)
		15300	$1.3^{+0.4}_{-0.3}$	(j)
	<i>R</i>	5655	$2.4^{+0.2}_{-0.2}$	(k)
		9255	$1.6^{+0.2}_{-0.1}$	(k)
	<i>r</i>	240	$2.1^{+0.4}_{-0.4}$	(i)
		15300	$1.1^{+0.3}_{-0.2}$	(j)
	<i>g</i>	240	$1.9^{+0.4}_{-0.3}$	(i)
150424A	<i>J</i>	57929	$14.7^{+2.8}_{-2.4}$	(l)
		62670	$11.8^{+2.3}_{-1.9}$	(l)
		67399	$10.2^{+2.4}_{-1.9}$	(l)
	<i>z</i>	57903	$11.1^{+0.6}_{-0.6}$	(l)

Table A.1: continued

GRB	Filter	δt^1 (sec)	Flux ² (μJy)	Reference ³
		62645	$10.0^{+0.5}_{-0.5}$	(l)
		67374	$9.0^{+0.5}_{-0.5}$	(l)
		156355	$3.3^{+0.4}_{-0.3}$	(l)
	<i>i</i>	57903	$9.5^{+0.5}_{-0.4}$	(l)
		62645	$9.6^{+0.4}_{-0.3}$	(l)
		67374	$8.5^{+0.4}_{-0.4}$	(l)
		156355	$2.2^{+0.3}_{-0.3}$	(l)
	<i>r</i>	57903	$8.7^{+0.2}_{-0.2}$	(l)
		62645	$8.3^{+0.2}_{-0.2}$	(l)
		67277	$6.9^{+0.2}_{-0.2}$	(l)
		156582	$2.1^{+0.1}_{-0.1}$	(l)
		323218	$0.98^{+0.22}_{-0.18}$	(l)
	<i>g</i>	57903	$7.2^{+0.3}_{-0.3}$	(l)
		62645	$6.3^{+0.2}_{-0.2}$	(l)
		67277	$5.8^{+0.2}_{-0.2}$	(l)
		156123	$1.7^{+0.2}_{-0.2}$	(l)
170428	<i>H</i>	3660	$15.8^{+7.1}_{-4.9}$	(m)
	<i>J</i>	3660	$19.1^{+3.9}_{-3.2}$	(m)
	<i>z</i>	3660	$13.2^{+1.3}_{-1.2}$	(m)
	<i>i</i>	3660	$13.2^{+1.3}_{-1.2}$	(m)
		91692	$5.2^{+2.3}_{-1.6}$	(n)
	<i>r</i>	3660	$11.0^{+1.1}_{-1.0}$	(m)
	<i>g</i>	3660	$10.0^{+1.0}_{-0.9}$	(m)

¹ Time since the trigger time (sec).

² If not specified, the flux is not corrected for extinctions of our galaxy or the host one in the direction of the GRB.

³ (a) Berger et al. (2005), (b) Malesani et al. (2007), (c) Soderberg et al. (2006), (d) Berger et al. (2009), (e) Fong et al. (2015) (f) Guelbenzu et al. (2012), (g) de Ugarte Postigo et al. (2014), (h) Troja et al. (2016), (i) Varela et al. (2015), (j) Littlejohns et al. (2015), (k) Kann et al. (2015), (l) Knust et al. (2017), (m) Bolmer et al. (2017), (n) Troja et al. (2017)

⁴ The fluxes are corrected for Galactic extinction in the direction of the GRB.

Table A.2: Results of spectral analysis for all model fit

GRB	Model	$N_{\text{H}}^{\text{rest}}$ (10^{21} cm^{-2})	$A_{\text{V}}^{\text{rest}}$ (mag)	β_{X}	E_{bk} (eV)	$\chi^2/(dof)$	Null hypothesis probability
050724	MW/po	< 0.21	< 0.12	$-0.74_{-0.01}^{+0.01}$	–	40 (31)	0.121
	LMC/po	< 0.21	< 0.19	$-0.74_{-0.01}^{+0.01}$	–	40 (31)	0.121
	SMC/po	< 0.21	< 0.21	$-0.74_{-0.01}^{+0.01}$	–	40 (31)	0.121
	MW/bknp0	< 0.39	$0.52_{-0.15}^{+0.15}$	$-0.87_{-0.06}^{+0.07}$	5_{-3}^{+12}	37 (30)	0.183
	LMC/bknp0	< 0.39	$0.51_{-0.15}^{+0.14}$	$-0.87_{-0.06}^{+0.07}$	5_{-3}^{+12}	37 (30)	0.182
	SMC/bknp0	< 0.39	$0.51_{-0.15}^{+0.15}$	$-0.87_{-0.06}^{+0.07}$	5_{-3}^{+12}	37 (30)	0.180
051221A	MW/po	$0.56_{-0.29}^{+0.31}$	$0.81_{-0.36}^{+0.37}$	$-0.83_{-0.06}^{+0.06}$	–	44 (46)	0.544
	LMC/po	$0.55_{-0.29}^{+0.31}$	$0.78_{-0.35}^{+0.35}$	$-0.83_{-0.06}^{+0.06}$	–	44 (46)	0.540
	SMC/po	$0.51_{-0.29}^{+0.30}$	$0.72_{-0.34}^{+0.34}$	$-0.82_{-0.05}^{+0.05}$	–	45 (46)	0.522
	MW/bknp0	$1.00_{-0.37}^{+0.40}$	< 1.02	$-0.95_{-0.08}^{+0.08}$	68_{-46}^{+153}	38 (45)	0.743
	LMC/bknp0	$0.99_{-0.23}^{+0.40}$	< 0.98	$-0.95_{-0.08}^{+0.09}$	65_{-53}^{+155}	38 (45)	0.743
	SMC/bknp0	$0.98_{-0.23}^{+0.41}$	< 0.88	$-0.94_{-0.08}^{+0.09}$	64_{-50}^{+157}	38 (45)	0.743
070724A	MW/po	$4.03_{-0.63}^{+0.73}$	$1.89_{-0.30}^{+0.31}$	$-0.77_{-0.02}^{+0.02}$	–	23 (19)	0.226
	LMC/po	$4.02_{-0.63}^{+0.73}$	$1.85_{-0.29}^{+0.31}$	$-0.77_{-0.02}^{+0.02}$	–	23 (19)	0.227
	SMC/po	$4.00_{-0.63}^{+0.73}$	$1.92_{-0.31}^{+0.33}$	$-0.77_{-0.02}^{+0.02}$	–	23 (19)	0.229
	MW/bknp0	$4.54_{-0.72}^{+1.20}$	$2.55_{-0.36}^{+0.33}$	$-0.85_{-0.05}^{+0.13}$	2_{-2}^{+14}	23 (18)	0.199
	LMC/bknp0	$4.54_{-0.71}^{+1.21}$	$2.49_{-0.36}^{+0.33}$	$-0.85_{-0.05}^{+0.13}$	2_{-2}^{+15}	23 (18)	0.199
	SMC/bknp0	$4.51_{-0.70}^{+1.26}$	$2.58_{-0.39}^{+0.33}$	$-0.84_{-0.08}^{+0.14}$	2_{-2}^{+17}	23 (18)	0.196
090510	MW/po	$1.53_{-0.26}^{+0.28}$	$0.07_{-0.07}^{+0.07}$	$-0.84_{-0.02}^{+0.02}$	–	107 (85)	0.051
	LMC/po	$1.53_{-0.26}^{+0.28}$	< 0.19	$-0.84_{-0.02}^{+0.02}$	–	108 (85)	0.049
	SMC/po	$1.53_{-0.26}^{+0.28}$	< 0.18	$-0.84_{-0.02}^{+0.02}$	–	108 (85)	0.050
	MW/bknp0	$1.53_{-0.26}^{+0.28}$	$0.07_{-0.07}^{+0.07}$	$-0.84_{-0.02}^{+0.02}$	*	107 (84)	0.043
	LMC/bknp0	$1.53_{-0.26}^{+0.28}$	< 0.19	$-0.84_{-0.02}^{+0.02}$	*	108 (84)	0.042
	SMC/bknp0	$1.53_{-0.26}^{+0.28}$	< 0.18	$-0.84_{-0.02}^{+0.02}$	*	108 (84)	0.043
130603B	MW/po	$2.43_{-0.22}^{+0.24}$	$0.79_{-0.05}^{+0.05}$	$-0.83_{-0.01}^{+0.01}$	–	58 (50)	0.206
	LMC/po	$2.42_{-0.22}^{+0.24}$	$0.76_{-0.05}^{+0.05}$	$-0.82_{-0.01}^{+0.01}$	–	57 (50)	0.218
	SMC/po	$2.39_{-0.22}^{+0.24}$	$0.72_{-0.05}^{+0.05}$	$-0.82_{-0.01}^{+0.01}$	–	56 (50)	0.253
	MW/bknp0	$2.99_{-0.36}^{+0.30}$	$1.14_{-0.10}^{+0.10}$	$-0.98_{-0.07}^{+0.08}$	8_{-6}^{+19}	48 (49)	0.498
	LMC/bknp0	$3.01_{-0.36}^{+0.38}$	$1.09_{-0.09}^{+0.09}$	$-0.98_{-0.07}^{+0.08}$	8_{-6}^{+21}	48 (49)	0.505

Table A.2: continued

GRB	Model	$N_{\text{H}}^{\text{rest}}$ (10^{21} cm^{-2})	$A_{\text{V}}^{\text{rest}}$ (mag)	β_{X}	E_{bk} (eV)	$\chi^2/(dof)$	Null hypothesis probability
140903A	SMC/bknp0	$3.10^{+0.42}_{-0.20}$	$0.99^{+0.09}_{-0.09}$	$-1.00^{+0.08}_{-0.07}$	15^{+38}_{-11}	49 (49)	0.477
	MW/po	$1.53^{+0.31}_{-0.28}$	$0.79^{+0.23}_{-0.24}$	$-0.80^{+0.03}_{-0.03}$	—	49 (39)	0.128
	LMC/po	$1.53^{+0.31}_{-0.28}$	$0.76^{+0.22}_{-0.23}$	$-0.80^{+0.03}_{-0.03}$	—	49 (39)	0.130
	SMC/po	$1.51^{+0.30}_{-0.27}$	$0.74^{+0.21}_{-0.22}$	$-0.79^{+0.03}_{-0.03}$	—	49 (39)	0.139
	MW/bknp0	$1.53^{+0.31}_{-0.28}$	$0.79^{+0.23}_{-0.24}$	$-0.80^{+0.03}_{-0.03}$	*	49 (38)	0.106
150423A	LMC/bknp0	$1.53^{+0.31}_{-0.28}$	$0.76^{+0.22}_{-0.23}$	$-0.80^{+0.03}_{-0.03}$	*	49 (38)	0.108
	SMC/bknp0	$1.51^{+0.30}_{-0.27}$	$0.74^{+0.21}_{-0.21}$	$-0.79^{+0.03}_{-0.03}$	*	49 (38)	0.116
	MW/po	$1.59^{+1.50}_{-1.17}$	< 0.55	$-0.76^{+0.03}_{-0.03}$	—	6 (7)	0.536
	LMC/po	$1.59^{+1.50}_{-1.17}$	< 0.57	$-0.76^{+0.03}_{-0.03}$	—	6 (7)	0.536
	SMC/po	$1.59^{+1.50}_{-1.17}$	< 0.56	$-0.76^{+0.03}_{-0.03}$	—	6 (7)	0.536
150424A	MW/bknp0	$1.59^{+1.50}_{-1.17}$	< 0.55	$-0.76^{+0.03}_{-0.03}$	*	6 (6)	0.419
	LMC/bknp0	$1.59^{+1.50}_{-1.17}$	< 0.57	$-0.76^{+0.03}_{-0.50}$	*	6 (6)	0.419
	SMC/bknp0	$1.59^{+1.50}_{-1.17}$	< 0.56	$-0.76^{+0.03}_{-0.03}$	*	6 (6)	0.419
	MW/po	< 0.09	< 0.03	$-0.76^{+0.01}_{-0.01}$	—	89 (47)	2.66e-02
	LMC/po	< 0.09	< 0.03	$-0.76^{+0.01}_{-0.01}$	—	89 (47)	2.66e-02
170428A	SMC/po	< 0.09	< 0.03	$-0.76^{+0.01}_{-0.01}$	—	89 (47)	2.66e-02
	MW/bknp0	$0.32^{+0.23}_{-0.22}$	< 0.15	$-1.01^{+0.06}_{-0.06}$	59^{+82}_{-34}	66 (46)	0.027
	LMC/bknp0	$0.32^{+0.23}_{-0.22}$	< 0.16	$-1.01^{+0.06}_{-0.06}$	59^{+82}_{-34}	66 (46)	0.027
	SMC/bknp0	$0.32^{+0.23}_{-0.22}$	< 0.15	$-1.01^{+0.06}_{-0.06}$	59^{+82}_{-34}	66 (46)	0.027
	MW/po	< 2.55	< 0.09	$-0.73^{+0.03}_{-0.02}$	—	8 (7)	0.344
170428A	LMC/po	< 2.55	< 0.06	$-0.73^{+0.03}_{-0.02}$	—	8 (7)	0.344
	SMC/po	< 2.55	< 0.06	$-0.73^{+0.03}_{-0.02}$	—	8 (7)	0.344
	MW/bknp0	< 3.72	< 0.28	$-0.92^{+0.16}_{-0.17}$	26^{+238}_{-23}	2 (6)	0.870
	LMC/bknp0	< 3.72	< 0.22	$-0.91^{+0.17}_{-0.15}$	20^{+247}_{-18}	3 (6)	0.869
	SMC/bknp0	< 3.72	< 0.21	$-0.92^{+0.16}_{-0.17}$	26^{+238}_{-23}	2 (6)	0.870

* Break energy are restricted by the lower limit we set.